Conditioned structure functions in turbulent hydrogen/air flames

Citation for the original published paper (version of record):
Sabelnikov, V., Lipatnikov, A., Nikolay, N. et al (2022). Conditioned structure functions in turbulent hydrogen/air flames. Physics of Fluids, 34(8). http://dx.doi.org/10.1063/5.0096509

Accepted to Phys. Fluids 10.1063/5.0096509

Conditioned structure functions in turbulent hydrogen/air flames

Vladimir A. Sabelnikov[a,*], Andrei N. Lipatnikov[b], Nikolay V. Nikitin[c], Francisco E. Hernández-Pérez[d], Hong G. Im[d]

[a]*ONERA – The French Aerospace Laboratory, F-91761 Palaiseau, France*
[b]*Department of Mechanics and Maritime Sciences, Chalmers University of Technology, Gothenburg, 41296 Sweden*
[c]*Lomonosov Moscow State University, Moscow, Russian Federation*
[d]*Clean Combustion Research Center, King Abdullah University of Science and Technology, Thuwal 23955-6900, Saudi Arabia*
*Corresponding author, sabelnikov@free.fr

Abstract

Direct numerical simulation data obtained from two turbulent, lean hydrogen-air flames propagating in a box are analyzed to explore the influence of combustion-induced thermal expansion on turbulence in unburned gas. For this purpose, Helmholtz-Hodge decomposition is applied to the computed velocity fields. Subsequently, the second-order structure functions conditioned to unburned reactants are sampled from divergence-free solenoidal velocity field or irrotational potential velocity field, yielded by the decomposition. Results show that thermal expansion significantly affects the conditioned potential structure functions not only inside the mean flame brushes, but also upstream of them. Upstream of the flames, firstly, transverse structure functions for transverse potential velocities grow with distance r between sampling points more slowly when compared to the counterpart structure functions sampled from the entire or solenoidal velocity field. Secondly, the former growth rate depends substantially on the distance from the flame-brush leading edge, even at small r. Thirdly, potential root-mean-square (rms) velocities increase with decreasing distance from the flame-brush leading edge and are comparable with solenoidal rms velocities near the leading edge. Fourthly, although the conditioned axial and transverse potential rms velocities are always close to one another, thus, implying isotropy of the potential velocity field in unburned reactants; the potential structure functions exhibit a high degree of anisotropy. Fifthly, thermal expansion effects are substantial even for the solenoidal structure functions and even upstream of a highly turbulent flame. These findings call for development of advanced models of turbulence in flames, which allow for the discussed thermal expansion effects.

***Keywords**:* Turbulent combustion; Thermal expansion; Helmholtz-Hodge decomposition; Structure functions

Accepted to Phys. Fluids 10.1063/5.0096509

I. INTRODUCTION

Substantial influence of combustion-induced thermal expansion on turbulence in flames has been known since the seminal papers by Karlovitz et al.[1] and Scurlock and Grover.[2] Over the past two decades, rapid development of Direct Numerical Simulation (DNS) methods and tools allowed researchers[3-9] to reveal various manifestations of this influence and to document significant changes of basic features of turbulence in premixed flames. Such results reviewed elsewhere[10-13] call for revisiting the problem of modeling turbulence in reacting flows. Although some DNS data indicate that certain combustion-induced thermal expansion effects are weakly pronounced in highly turbulent flames,[14-21] these data do not deny the need for advancing models of turbulence in flames. Indeed, firstly, there is no widely recognized criterion for assessing importance of the combustion-induced thermal expansion effects under specific conditions. Secondly, weak influence of the thermal expansion on certain turbulence characteristics does not prove that all other turbulence characteristics are also weakly affected by the thermal expansion under the same conditions. For instance, recent experimental data[22,23] obtained from highly turbulent lean methane-air swirl flames show importance of thermal expansion effects such as vorticity generation due to baroclinic torque[22] or back-scatter.[23]

Thus, there is a clear need for development of an advanced model of turbulence in flames, which could predict phenomena revealed recently and reviewed elsewhere.[10-13] However, no comprehensive modeling framework to represent distinct roles of thermal expansion on turbulence exists today. To develop such a framework, more knowledge about the influence of combustion-induced thermal expansion on turbulence is required first. For this reason, a set of methods applied to explore this influence was greatly extended recently.[10-13,17-21] In particular, the joint use of conditioned structure function (SF) techniques[17,24-26] and Helmholtz-

Hodge decomposition[27] (HHD) appears to be a promising tool for acquiring fundamental knowledge on turbulence in flames. The present work aims at applying this newly introduced research tool[28] to DNS data of two turbulent lean H_2/air flames with detailed chemistry.[21,29-31]

In the next section, research methods are presented. Results are reported and discussed in Sect. III, followed by conclusions.

II. RESEARCH METHODS

A. Helmholtz-Hodge decomposition

HHD is a decomposition of a fluctuating velocity field $\mathbf{u}'(\mathbf{x},t)$ into two subfields: (i) divergence-free solenoidal subfield $\mathbf{u}'_s(\mathbf{x},t)$ and (ii) curl-free potential subfield $\mathbf{u}'_p(\mathbf{x},t)$, i.e.,

$$\mathbf{u}' = \mathbf{u}'_s + \mathbf{u}'_p, \quad \nabla\cdot\mathbf{u}'_s = 0, \quad \nabla\times\mathbf{u}'_p = 0. \tag{1}$$

The last equality holds if $\mathbf{u}'_p = \nabla\varphi$, where $\varphi(\mathbf{x},t)$ is an arbitrary scalar function with $\Delta\varphi = \nabla\cdot\mathbf{u}'_p = \nabla\cdot\mathbf{u}'$ due to Eq. (1). HHD is of particular value for exploring the influence of thermal expansion on the generation of potential velocity fluctuations in flames.

In the present work, two HHD methods were used: (i) conventional HHD[27] and (ii) natural decomposition.[32,33] The former decomposition invokes the following constraint

$$\iiint_V \mathbf{u}'_s\cdot\mathbf{u}'_p d\mathbf{x} = 0, \tag{2}$$

which guarantees the additivity of the bulk kinetic energies of the solenoidal and potential flow fields, i.e.

$$\iiint\limits_V \mathbf{u}'\cdot\mathbf{u}' d\mathbf{x} = \iiint\limits_V \mathbf{u}'_s\cdot\mathbf{u}'_s d\mathbf{x} + \iiint\limits_V \mathbf{u}'_p\cdot\mathbf{u}'_p d\mathbf{x}. \tag{3}$$

Here, V designates the computational domain. Substitution of Eq. (1) into Eq. (2) yields

$$\iiint\limits_V \mathbf{u}_s' \cdot \nabla\varphi d\mathbf{x} = \iiint\limits_V \nabla(\varphi\mathbf{u}_s') d\mathbf{x} - \iiint\limits_V \varphi\nabla\cdot\mathbf{u}_s' d\mathbf{x} = \oiint\limits_S \varphi\mathbf{u}_s'\cdot\mathbf{n}dS - \iiint\limits_V \varphi\nabla\cdot\mathbf{u}_s' d\mathbf{x}. \quad (4)$$

Here, S is the boundary of the domain V and the unit vector $\mathbf{n}$ is normal to this boundary. The second (volume) integral vanishes, because $\nabla\cdot\mathbf{u}_s = 0$. The first (surface) integral vanishes if $\mathbf{u}_s\cdot\mathbf{n} = 0$. In this case, Eq. (2) holds and

$$\left.\frac{\partial\varphi}{\partial n}\right|_S = \mathbf{n}\cdot\nabla\varphi|_S = \mathbf{n}\cdot\mathbf{u}|_S \quad (5)$$

on the boundary S. The Neumann problem given by $\Delta\varphi = \nabla\cdot\mathbf{u}'$ and Eq. (5) has a unique solution for $\varphi(\mathbf{x},t)$, i.e., the use of Eq. (2) or (5) makes the HHD unique.

The natural decomposition[32,33] deals with an extra vector-field $\mathbf{w}(\mathbf{x},t)$, defined as follows: (i) $\mathbf{w}(\mathbf{x},t) = \mathbf{u}(\mathbf{x},t)$ for all $\mathbf{x}\in V$, and (ii) $\mathbf{w}(\mathbf{x},t)$ is extrapolated to the entire 3D space $\mathbb{R}^3$ such that $|\mathbf{w}(\mathbf{x},t)| \to 0$ for $|\mathbf{x}|\to\infty$. This velocity field $\mathbf{w}(\mathbf{x},t)$ can be decomposed in the entire space, i.e.,

$$\mathbf{w} = \nabla\Gamma + \nabla\times\mathbf{S}, \qquad \mathbf{x}\in\mathbb{R}^3, \quad (6)$$

$$\Delta\Gamma = \nabla\cdot\mathbf{w}, \qquad \mathbf{x}\in\mathbb{R}^3, \quad (7)$$

$$\nabla\times\nabla\times\mathbf{S} = \nabla\times\mathbf{w}, \qquad \mathbf{x}\in\mathbb{R}^3. \quad (8)$$

Solutions to Eqs. (7)-(8) are unique

$$\Gamma(\mathbf{x}_0,t) = \iiint\limits_{\mathbb{R}^3} G_\infty(\mathbf{x},\mathbf{x}_0)\nabla\cdot\mathbf{w}(\mathbf{x},t)d\mathbf{x}, \qquad \mathbf{x}_0,\mathbf{x}\in\mathbb{R}^3, \quad (9)$$

$$\mathbf{S}(\mathbf{x}_0,t) = -\iiint\limits_{\mathbb{R}^3} G_\infty(\mathbf{x},\mathbf{x}_0)\nabla\times\mathbf{w}(\mathbf{x},t)d\mathbf{x}, \qquad \mathbf{x}_0,\mathbf{x}\in\mathbb{R}^3. \quad (10)$$

where $G_\infty(\mathbf{x},\mathbf{x}_0) = -1/(4\pi|\mathbf{x}-\mathbf{x}_0|)$ is the free-space Green's function in $\mathbb{R}^3$. Then, integration in Eqs. (9)-(10) can be truncated outside the domain V by interpreting the truncated integrals to be an external influence. Therefore,

$$\Gamma^*(\mathbf{x}_0,t) = \iiint\limits_V G_\infty(\mathbf{x},\mathbf{x}_0)\nabla\cdot\mathbf{u}(\mathbf{x},t)d\mathbf{x}, \qquad \mathbf{x}_0,\mathbf{x}\in V, \tag{11}$$

$$\mathbf{S}^*(\mathbf{x}_0,t) = -\iiint\limits_V G_\infty(\mathbf{x},\mathbf{x}_0)\nabla\times\mathbf{u}(\mathbf{x},t)d\mathbf{x}, \qquad \mathbf{x}_0,\mathbf{x}\in V. \tag{12}$$

Equation (1) with $\mathbf{u}_s = \nabla\times\mathbf{S}^*$ and $\mathbf{u}_p = \nabla\Gamma^*$ holds due to Eqs. (6)-(8).

Results yielded by the two HHD methods were compared in detail in an earlier paper.[28] Since these results are hardly distinguishable within flame brushes, we will report results obtained using the conventional HHD only.

B. Conditioned structure functions

In fluid mechanics, the second-order SFs of a velocity field form the following tensor[35]

$$D_{ij}(\mathbf{x},\mathbf{r}) \equiv \overline{[u_i(\mathbf{x}+\mathbf{r},t)-u_i(\mathbf{x},t)][u_j(\mathbf{x}+\mathbf{r},t)-u_j(\mathbf{x},t)]}, \tag{13}$$

where overbar designates averaging; u_i and u_j are i-th and j-th components, respectively, of the velocity vector $\mathbf{u} = \{u,v,w\}$. Similarly to the turbulence spectrum, such SFs characterize the distribution of turbulent energy over spatial scales.[35] Accordingly, the SFs are widely used to study turbulence since a seminal work by Kolmogorov[36] and to model unresolved small-scale effects in Large Eddy Simulations.[37]

When Eq. (13) is applied to a flame, the velocity differences are controlled not only by turbulence, but also by thermal expansion effects. Such effects can be of primary importance if the local flame front is between the points $\mathbf{x}$ and $\mathbf{x}+\mathbf{r}$. Therefore, additional considerations are needed to use SFs in combustion research. To this end, conditioned SFs were independently introduced by Whitman et al.[17] and by Sabelnikov et al.[24,25] They applied two different methods to DNS data of highly[17] and weakly[24,25] turbulent single-step chemistry flames. Subsequently, the latter method was adopted[26] to analyze DNS data of single-step chemistry flames, characterized by various ratios $1 \leq u'/S_L \leq 10$ of root-mean-square (rms) velocity, u', to the laminar flame speed, S_L. Later, conditioned SFs were jointly used with HHD[28] to explore thermal expansion effects in weakly turbulent single-step chemistry flames. Yet, neither application of conditioned SFs to complex chemistry turbulent flames nor joint application of conditioned SFs and HHD to moderately or highly turbulent combustion has been reported.

Here, the conditioned second-order SFs of the velocity field are defined as follows[24,25]

$$D_{ij}^{\alpha\beta}(\mathbf{x},\mathbf{r}) \equiv \frac{1}{\mathrm{P}_{\alpha\beta}} \overline{[u_i(\mathbf{x}+\mathbf{r},t)-u_i(\mathbf{x},t)][u_j(\mathbf{x}+\mathbf{r},t)-u_j(\mathbf{x},t)]I_\alpha(\mathbf{x},t)I_\beta(\mathbf{x}+\mathbf{r},t)}, \quad (14)$$

where superscripts α and β refer to the mixture state; the indicator function $I_u(\mathbf{x},t)$ is equal to unity if reactants are observed in point $\mathbf{x}$ at instant t and vanishes otherwise; $I_b(\mathbf{x},t) = 1$ if products are observed in point $\mathbf{x}$ at instant t and vanishes otherwise; $I_r(\mathbf{x}) = 1$ if $I_u(\mathbf{x},t) = I_b(\mathbf{x},t) = 0$ and vanishes otherwise; and $\mathrm{P}_{\alpha\beta} = \overline{I_\alpha(\mathbf{x},t)I_\beta(\mathbf{x}+\mathbf{r},t)}$ are probabilities that the mixture states α and β are recorded in points $\mathbf{x}$ and $\mathbf{x}+\mathbf{r}$, respectively, at the same instant.

Depending on α and β, there are different conditioned SF tensors, with $D_{ij}(\mathbf{x},\mathbf{r})$ being equal to $\sum_{\alpha=1}^{3}\sum_{\beta=1}^{3} D_{ij}^{\alpha\beta}(\mathbf{x},\mathbf{r})$ due to the identity of $\sum_{\alpha=1}^{3}\sum_{\beta=1}^{3} I_\alpha(\mathbf{x})I_\beta(\mathbf{x}+\mathbf{r}) = 1$. The present work is restricted to the conditioned SFs D_{ij}^{uu} sampled in the cases where both $\mathbf{x}$ and $\mathbf{x}+\mathbf{r}$ are in the unburned gas. Such conditioned SFs appear to be of the most interest because (i) a flame propagates into unburned gas and (ii) the velocity field upstream of the flame plays a key role in the flame acceleration. Henceforth, the superscript *uu* will be omitted for brevity.

Since the DNS data analyzed here were obtained from statistically one-dimensional and planar flames propagating from right to left along the x-direction in a box, the flow field is assumed to be statistically isotropic and homogeneous in any plane x =const. Hence, the present study is restricted to SFs found for points $\mathbf{x} = \{x, y, z\}$ and $\mathbf{x} = \{x, y + r_y, z + r_z\}$ that belong to the same transverse plane x = const, i.e., $\mathbf{r} = \{0, r_y, r_z\}$.

C. Numerical simulations and data analysis

As the DNS were discussed earlier,[29-31] only a brief description is given here. Lean (the equivalence ratio Φ=0.7) H_2-air turbulent flames propagating in a box were investigated by (i) adopting a detailed (9 species, 23 reversible reactions) chemical mechanism[38] with the mixture-averaged transport model and (ii) numerically solving unsteady three-dimensional governing equations written in compressible form.

Along the flame propagation direction x, inflow and outflow characteristic boundary conditions were set. Other boundaries were periodic. A divergence-free, isotropic, homogeneous turbulent velocity field was generated using a pseudo spectral method[39] and adopting the Passot-Pouquet spectrum.[40] The field was injected through the inlet (left) boundary and decayed along the mean flow direction (x-axis).

TABLE I. Relevant parameters characterizing the DNS cases

	u'/S_L	L_T/δ_L	Re_T	Da	Ka_1	Ka_2
W	0.7	14	227	20	33	0.5
H	5.0	14	1623	2.8	270	4

Ratios of the inflow value of the rms velocity to S_L, ratios of the most energetic length scale L_T of the Passot-Pouquet spectrum to the laminar flame thickness $\delta_L = (T_b - T_u)/\max|\nabla T|$, turbulent Reynolds number $Re_T = u'L_T/\nu_u$, Damköhler number $Da = L_T S_L/(u'\delta_L)$, and two Karlovitz numbers are reported for the studied flames in Table 1. Here, $S_L = 1.36$ m/s and $\delta_L = 0.36$ mm have been computed using the same chemical mechanism under the simulation conditions (temperature $T_u = 300$ K and pressure $P = 1$ atm); ν_u is the kinematic viscosity of unburned gas; $Ka_1 = (\delta_L/\eta_K)^2$ and $Ka_2 = \delta_L/(S_L\tau_K)$ have been evaluated using (i) the Kolmogorov length scale $\eta_K = \nu_u^{3/4}\bar{\varepsilon}^{-1/4}$ and time scale $\tau_K = \nu_u^{1/2}\bar{\varepsilon}^{-1/2}$, (ii) the dissipation rate $\bar{\varepsilon} = 2\overline{\nu S_{ik}S_{ik}}$ averaged over the leading edge ($\bar{c} = 0.01$, with the combustion progress variable c being defined using fuel mass fraction) of the mean flame brush, and (iii) the rate-of-strain tensor $S_{ik} = 0.5(\partial u_i/\partial x_k + \partial u_k/\partial x_i)$.

The number Ka_1 is significantly larger than Ka_2, because $\delta_L = (T_b - T_u)/\max|\nabla T| \gg \nu_u/S_L$ for the lean hydrogen-air laminar flame addressed here. Since (i) thicknesses of preheat and reaction zones are comparable in this flame and (ii) Ka_1 is large; both cases W and H are associated with a significant probability of penetration of small-scale turbulent eddies into local reaction zones.[41] Since $Ka_2 > 1$ in flame H, it is also associated with substantial probability of local combustion quenching.[41] Thus, as far as the influence of turbulence on combustion is concerned, case H is definitely associated with highly turbulent burning. Nevertheless, even in this case, the influence of combustion on turbulence can be significant, as shown in Sect. III.

When analyzing the DNS data, firstly, transverse-averaged quantities $\langle q\rangle(x,t)$ were sampled at each instant. Secondly, these x-dependencies were mapped to $\langle c\rangle$-dependencies using the averaged profiles $\langle c\rangle(x,t)$. Thirdly, mean values $\bar{q}(\bar{c})$ of the quantity q, e.g., a product of velocity differences in Eq. (14), were found by averaging $\langle q\rangle[\langle c\rangle(x,t)]$ over time.

The probability $\mathrm{P}_{uu}(x,r)$ and the conditioned SFs determined by Eq. (14) were sampled from points characterized by $c(\mathbf{x},t) < \epsilon \ll 1$, with three such SFs being considered. Firstly, the transverse SFs $D_{xx,T}(x,r)$ for the axial velocity u' were computed by sampling $[u'(\mathbf{x}+\mathbf{r},t) - u'(\mathbf{x},t)]^2$ from two sets of points: (i) $\mathbf{r} = \{0,r,0\}$ and (ii) $\mathbf{r} = \{0,0,r\}$.

Subsequently, the two samples were averaged. Secondly, the transverse SFs $D_{yz,T}(x,r)$ for the transverse velocities v and w were obtained by sampling (i) $[v'(\mathbf{x}+\mathbf{r},t)-v'(\mathbf{x},t)]^2$ from points characterized by $\mathbf{r}=\{0,0,r\}$ and (ii) $[w'(\mathbf{x}+\mathbf{r},t)-w'(\mathbf{x},t)]^2$ from points characterized by $\mathbf{r}=\{0,r,0\}$. Subsequently, the two samples were averaged. Thirdly, the longitudinal SFs $D_{yz,L}(x,r)$ for the transverse velocities were found by sampling (i) $[v'(\mathbf{x}+\mathbf{r},t)-v'(\mathbf{x},t)]^2$ from points characterized by $\mathbf{r}=\{0,r,0\}$ and (ii) $[w'(\mathbf{x}+\mathbf{r},t)-w'(\mathbf{x},t)]^2$ from points characterized by $\mathbf{r}=\{0,0,r\}$. Subsequently, the two samples were averaged. Solenoidal and potential conditioned SFs were obtained by separately applying such diagnostics to the solenoidal and potential velocity subfields, respectively.

Reported in the following are dependencies of the conditioned SFs on the distance r, sampled either inside a flame brush at various $\bar{c}(x)$ or upstream of a flame brush at various distances Δx from it. The SFs were sampled adopting the threshold $\epsilon = 0.05$ and the combustion progress variable $c = 1 - Y_F/Y_{F,u}$ defined using fuel mass fraction. Weak sensitivity of the obtained results to ϵ (either 0.01 or 0.05) or to the choice of combustion progress variable (temperature, water, and oxygen-based combustion progress variables were also adopted to analyze the same DNS data[30]) was checked.

III. RESULTS AND DISCUSSION

Figure 1 shows normalized transverse SFs $D_{xx,T}[\bar{c}(x),r]$ for the total, solenoidal, and potential fluctuating axial velocity fields, conditioned to unburned gas in flames W (top row) and H (bottom row). The SFs have been sampled from various transverse planes characterized by different $\bar{c}$ (see the figure legends). Henceforth, (i) each subfigure that reports a SF contains an insert, which sketches the SF type, and (ii) total, solenoidal, and potential SFs are normalized using conditioned total, solenoidal, and potential rms velocities, respectively, which are reported in Fig. 2.

At first glance, Figs. 1a and 1d do not show any significant and systematic change of the total SF $D_{xx,T}[\bar{c}(x),r]$ with $\bar{c}$ if $\bar{c} \leq 0.25$. Such changes are not observed for the solenoidal SFs either (Figs. 1b and 1e). Concerning the differences between $D_{xx,T}[\bar{c}(x),r]$ sampled at $\bar{c} \leq 0.25$ and $\bar{c} = 0.5$ (red dotted-dashed lines), they can be attributed to decorrelation of unburned gas motion in two points on the opposite sides of a flame segment. The probability of finding such pairs of points is increased with the distance r and with $\bar{c}$, thus, making the $D_{xx,T}[\bar{c} = 0.5,r]$-curves less smooth at $r > \delta_L$.

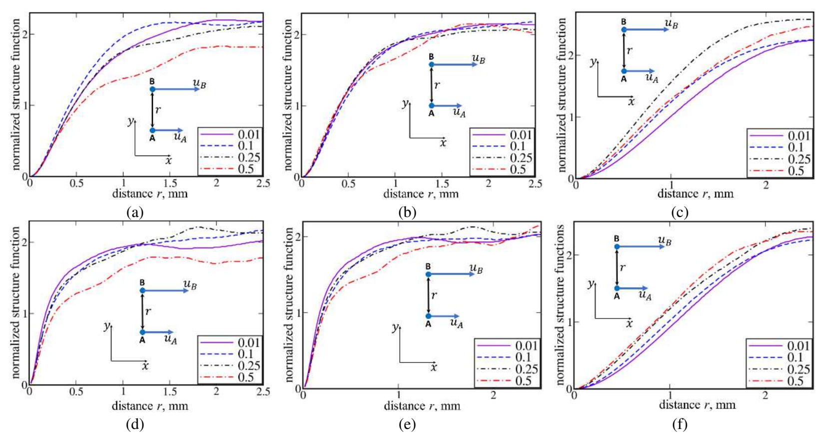

FIG. 1. Normalized transverse structure functions for the axial velocity, conditioned to unburned gas and sampled from different transverse planes in flames W (top row) and H (bottom row). Values of Reynolds-averaged combustion progress variable characterizing sampling planes are reported in the legends. Results obtained by analyzing (a) and (d) total, (b) and (e) solenoidal, or (c) and (f) potential velocity fields are reported in the left, middle, and right columns, respectively. $\delta_L = 0.36$ mm.

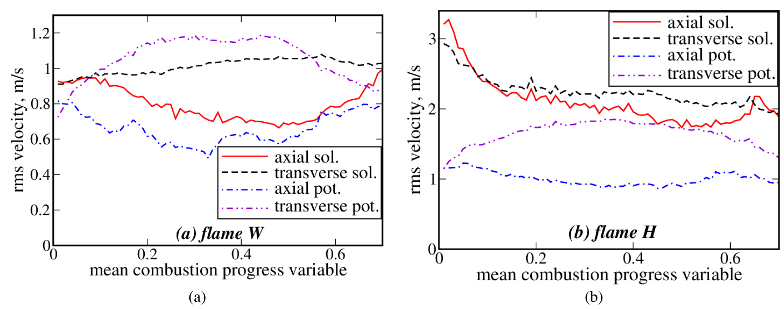

FIG. 2. Variations of conditioned (i) axial solenoidal and potential rms velocities $\langle u_s'^2 | c(\mathbf{x},t) < 0.05\rangle^{1/2}$ and $\langle u_p'^2 | c(\mathbf{x},t) < 0.05\rangle^{1/2}$, respectively, and (ii) transverse solenoidal and potential rms velocities $\langle 0.5(v_s'^2 + w_s'^2) | c(\mathbf{x},t) < 0.05\rangle^{1/2}$ and $\langle 0.5(v_p'^2 + w_p'^2) | c(\mathbf{x},t) < 0.05\rangle^{1/2}$, respectively, in flames (a) W and (b) H.

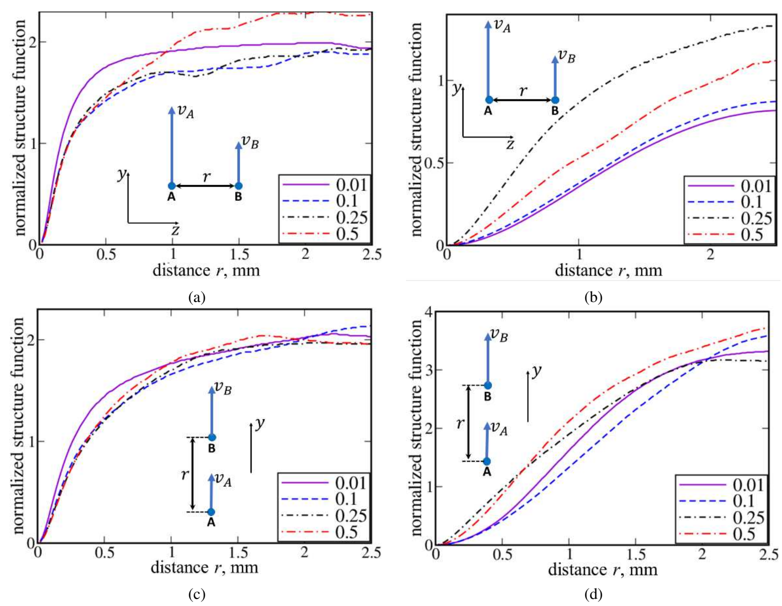

FIG. 3. Normalized (a) and (b) transverse structure functions $D_{yz,T}[\bar{c}(x), r]$ (top row) or (c) and (d) longitudinal structure functions $D_{yz,L}[\bar{c}(x), r]$ (bottom row) for the transverse velocities, conditioned to unburned gas and sampled from different transverse planes in flame H. Values of Reynolds-averaged combustion progress variable characterizing sampling planes are reported in the legends. Results obtained by analyzing (a) and (c) total or (b) and (d) potential fluctuating velocity fields are reported in the left and right columns, respectively. $\delta_L = 0.36$ mm.

On the contrary, the potential SF $D_{xx,T}[\bar{c}(x),r]$ is increased with $\bar{c}$ at $\bar{c} \leq 0.25$ (Figs. 1c and 1f). The trend is well pronounced in case W (Fig. 1c). Even in the highly turbulent flame H (Fig. 1f), the trend is evident, but variations in $D_{xx,T}[\bar{c}(x),r]$ with $\bar{c}$ are less pronounced, thus indicating some reduction of the magnitude of thermal expansion effects in more intense turbulence. Moreover, the increase in the potential SF $D_{xx,T}[\bar{c}(x),r]$ with $\bar{c}$ (at $\bar{c} \leq 0.25$) is evident at various distances r, including small distances $r < \delta_L$. Thus, Figs. 1c and 1f clearly indicate substantial influence of combustion-induced thermal expansion on all scales of potential velocity fluctuations in unburned gas within the mean flame brush. While the potential SFs are normalized using the potential rms velocities, Fig. 2 shows that the potential and solenoidal axial rms velocities are comparable in magnitude in flame W or H.

Significant variations of the conditioned potential SFs $D_{yz,T}[\bar{c}(x),r]$ and $D_{yz,L}[\bar{c}(x),r]$ with $\bar{c}$ are also seen in both cases, including the highly turbulent flame H (see Figs. 3b and 3d, where such variations are strongly pronounced for $0.1 \leq \bar{c} \leq 0.25$, especially for $D_{yz,T}[\bar{c}(x),r]$). Again, differences between the conditioned potential SFs $D_{yz,T}[\bar{c}(x),r]$ or $D_{yz,L}[\bar{c}(x),r]$ sampled at different $\bar{c}$ are significant even at small distance $r < \delta_L$. Moreover, comparison of Figs. 3a and 3b or Figs. 3c and 3d shows an important qualitative difference between the total (left column in Fig. 3) and potential (right column) SFs; the potential SFs increase significantly slower with distance r and do not level off even at large r. The same qualitative difference is observed when comparing Figs. 1a and 1c or Figs. 1d and 1f.

As shown above, the spatial structure of potential velocity fluctuations differs substantially from that of the incoming solenoidal turbulent fluctuations. Such changes of the spatial structure of the fluctuating velocity field in unburned gas within flame brush are not negligible, because conditioned solenoidal and potential rms velocities are of the same order even in the highly turbulent flame H (Fig. 2b). Also note that the conditioned total SFs

$D_{yz,T}[\bar{c}(x), r]$ and $D_{yz,L}[\bar{c}(x), r]$ sampled at $\bar{c} = 0.01$ differ from their counterparts sampled at $0.1 \leq \bar{c}$, even at small distance $r < \delta_L$ (Figs. 3a and 3c), further indicating the importance of the influence of thermal expansion on turbulence in flames.

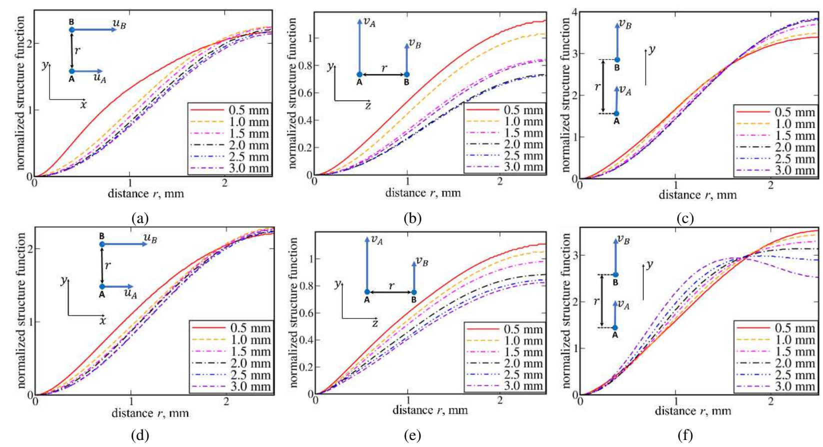

FIG. 4. Normalized potential structure functions (a) and (d) $D_{xx,T}(x,r)$ (left column), (b) and (e) $D_{yz,T}(x,r)$ (middle column), or (c) and (f) $D_{yz,L}(x,r)$ (right column) sampled upstream of flames (a-c) W (top row) and (d-f) H (bottom row) at different distances from their leading edges, specified in the legends. $\delta_L = 0.36$ mm.

For the potential velocity field, such an influence is well pronounced even upstream ($\bar{c} < 0.01$) of the flame brushes in both cases (Fig. 4), with the field being highly anisotropic. Indeed, on the one hand, variations of potential SFs with the distance Δx (see legends) from the flame leading edge are most pronounced for $D_{yz,T}(x,r)$ (Figs. 4b and 4e) and least pronounced for $D_{yz,L}(x,r)$ (Figs. 4c and 4f). On the other hand, at large r, $D_{yz,L}(x,r)$ is significantly larger than $D_{yz,T}(x,r)$. Moreover, the anisotropy of the potential SFs is significantly more pronounced than the weak anisotropy of potential rms velocities (Fig. 5), which were used to normalize the SFs. This demonstrates that simple diagnostic tools (rms velocities) are unable to reveal the explored thermal expansion effects.

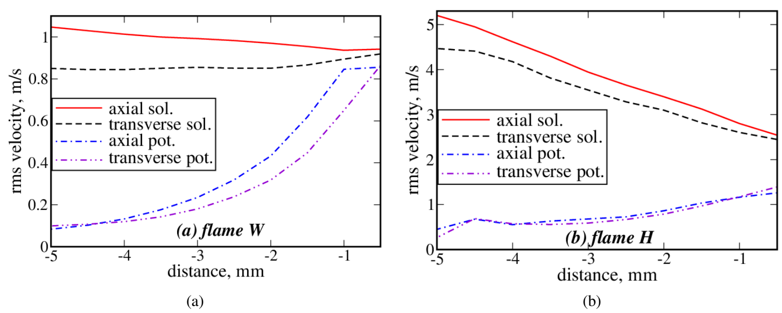

FIG. 5. Variations of (i) axial solenoidal and potential rms velocities $\left(\overline{u_s'^2}\right)^{1/2}$ and $\left(\overline{u_p'^2}\right)^{1/2}$, respectively, and (ii) transverse solenoidal and potential rms velocities $\left[0.5\overline{\left(v_s'^2+w_s'^2\right)}\right]^{1/2}$ and $\left[0.5\overline{\left(v_p'^2+w_p'^2\right)}\right]^{1/2}$, respectively, upstream of flames (a) W and (b) H.

Comparison of Figs. 4a and 4d or 4b and 4e indicates that variations in the potential transverse structure function $D_{xx,T}(x,r)$ or $D_{yz,T}(x,r)$, respectively, with Δx are more pronounced in flame W, thus, again implying some reduction of the magnitude of thermal expansion effects in more intense turbulence. However, comparison of Figs. 4c and 4f shows the opposite trend for the potential longitudinal structure function $D_{yz,L}(x,r)$.

Figure 4 also shows that the potential SFs $D_{yz,T}(x,r)$ and $D_{yz,L}(x,r)$ do not approach 2 at large r. To the contrary, in homogeneous turbulence, $D_{ii}(\mathbf{r}) = 2\overline{u_i'^2}$ at large distances $|\mathbf{r}|$ because the correlation between velocities vanishes.[35] Thus, Fig. 4 indicates that combustion-induced transverse velocity fluctuations correlate at large distances. Difference between transverse velocities $v(x,y,z,t)$ and $v(x,y+r,z,t)$ could be statistically positive even at large r, because thermal expansion in a flame tongue can push unburned gas to the opposite directions on the opposite sides of the tongue. As a result, within a flame brush, $D_{yz,L}(x,r)$ could be significantly larger than 2 at large r (Fig. 3d). Figures 4c and 4f imply that such flow perturbations can expand upstream of a flame brush due to pressure waves.

Figure 5 shows that, upstream of a flame brush, the potential rms velocity increases with decreasing distance from the flame leading edge (from left to right), with the effect being more pronounced in case W. As a result, potential and solenoidal rms velocities are almost equal or, at least, comparable at $|\Delta x| = 0.5$ mm in case W or H, respectively. While comparable magnitudes of the potential and solenoidal rms velocities at $|\Delta x| = 0.5$ mm in case H stem partially from the spatial decay of the solenoidal velocity fluctuations, the Karlovitz numbers reported in Table 1 have been evaluated using the dissipation rate $\bar{\varepsilon}$ sampled at $|\Delta x| = 0$. Thus, despite the turbulence decay, case H deals with a highly turbulent flame. Moreover, even if an increase in the potential rms velocities with decreasing $|\Delta x|$ seems to be more pronounced in flame W, these rms velocities are larger in case H at $|\Delta x| = 0$.

The simulated influence of combustion-induced thermal expansion on turbulence upstream of a premixed flame brush is not unexpected. This effect stems from rapid propagation of pressure perturbations from the flame to upstream flow of unburned reactants. In a laminar flow, such pressure perturbations are well known to cause hydrodynamic instability of a laminar premixed flame,[42] or self-similar acceleration of a large-scale flame kernel ignited in a quiescent mixture.[43] In turbulent flows, some influence of a premixed flame on upstream turbulence was documented in a few experimental papers,[44,45] but the phenomenon requires more studies. It has not yet been explored by another research group by analyzing DNS data obtained from premixed turbulent flames or by adopting HHD techniques.

Finally, Fig. 6 shows that even solenoidal SFs sampled upstream of flame H vary with the distance $|\Delta x|$, with the effect being most pronounced at $\delta_L < r < 3\delta_L$ and $|\Delta x| \leq 1$ mm. A flame can affect the upstream solenoidal velocity field due to the potential velocity contribution to vortex-stretching term in vorticity transport equation,[10-13] but such secondary effects are less pronounced than the direct influence of combustion-induced pressure perturbations on the potential velocity.

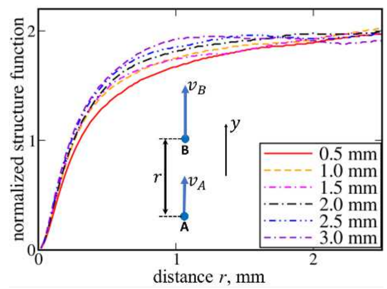

FIG. 6. Normalized solenoidal structure functions $D_{yz,L}(x,r)$ sampled upstream of flame H.

IV. CONCLUSIONS

Two advanced research tools, (i) Helmholtz-Hodge decomposition of fluctuating velocity into divergence-free solenoidal and irrotational potential components and (ii) conditioned structure functions, were jointly used to explore the influence of combustion-induced thermal expansion on turbulence by analyzing DNS data of complex chemistry, lean H_2/air, turbulent flames. While these two methods were earlier[28] applied to explore such an influence, the major advancement of the present work consists of showing importance of thermal expansion effects in highly turbulent flames. Moreover, the present analysis has yielded new insights into the influence of thermal expansion on turbulence, as follows.

Firstly, results show that thermal expansion effects can seem to be weakly pronounced when analyzing conditioned SFs for the entire or solenoidal velocity field, but well pronounced when exploring potential SFs. Moreover, while the potential SFs clearly show significant anisotropy of velocity field upstream of flame brush, such a trend is not revealed when analyzing the potential rms velocities. Thus, the use of a single diagnostic technique is not sufficient to prove that thermal expansion effects are of minor importance.

Secondly, under conditions of the present study, thermal expansion substantially changes not only SFs conditioned to unburned gas within mean flame brush, but also SFs sampled upstream of the flame brush. Such effects are more pronounced for the potential SFs but are also notable for the solenoidal SFs. These results show that a premixed flame is stretched by turbulence that differs substantially from turbulence far upstream of the flame. While the documented effects of combustion-induced thermal expansion on the flow are more pronounced in the flame W associated with a less intense turbulence, they play a role in the highly turbulent flame H as well.

The reported findings call for development of advanced models of turbulence in flames, which allow for the discussed thermal expansion effects and can predict them at least qualitatively. The joint use of HHD and conditioned SF methods appears to be a promising tool for acquiring fundamental knowledge that is required for development of such models. Since comparison of the present results obtained from complex-chemistry moderately and highly turbulent flames with results obtained earlier[28] from two single-step-chemistry weakly turbulent flames does not reveal any significant effect resulting from complex combustion chemistry, it is recommended to perform future DNS studies of the influence of premixed combustion on turbulence by employing simpler chemical kinetic mechanisms in favor of computational efficiency to cover a wider range of turbulent flame characteristics (u'/S_L, L_T/δ_L, Ka, Da, Re_T, etc.). On the contrary complex chemistry effects should be addressed when exploring the influence of turbulence on combustion.

ACKNOWLEDGEMENTS

VAS gratefully acknowledges the financial support provided by ONERA. ANL gratefully acknowledges the financial support provided by Combustion Engine Research Center (CERC). FEHP and HGI were sponsored by King Abdullah University of Science and

Technology (KAUST). Computational resources for the DNS calculations were provided by the KAUST Supercomputing Laboratory.

AUTHOR DECLARATIONS

Conflict of Interest

The authors have no conflicts to disclose.

DATA AVAILABILITY

The data that support the findings of this study are available from the corresponding author upon reasonable request.

REFERENCES

[1]B. Karlovitz, D. W. Denniston, and F. E. Wells, "Investigation of turbulent flames," J. Chem. Phys. **19**, 541 (1951).
[2]A. C. Scurlock and J. H. Grover, "Propagation of turbulent flames," Proc. Combust. Inst. **4**, 645 (1953).
[3]C. Dopazo, L. Cifuentes, and N. Chakraborty, "Vorticity budgets in premixed combusting turbulent flows at different Lewis numbers," Phys. Fluids **29**, 045106 (2017).
[4]A. N. Lipatnikov, V. A. Sabelnikov, S. Nishiki, and T. Hasegawa, "Combustion-induced local shear layers within premixed flamelets in weakly turbulent flows," Phys. Fluids **30**, 085101 (2018).
[5]A. N. Lipatnikov, V. A. Sabelnikov, S. Nishiki, and T. Hasegawa, "Does flame-generated vorticity increase turbulent burning velocity?" Phys. Fluids **30**, 081702 (2018).
[6]A. N. Lipatnikov, V. A. Sabelnikov, S. Nishiki, and T. Hasegawa, "A direct numerical simulation study of the influence of flame-generated vorticity on reaction-zone-surface area in weakly turbulent premixed combustion" Phys. Fluids **31**, 055101 (2019).
[7]A. R. Varma, U. Ahmed, and N. Chakraborty "Effects of body forces on vorticity and enstrophy evolutions in turbulent premixed flames," Phys. Fluids **33**, 035102 (2021).
[8]J. F. MacArt and M. E. Mueller, "Damköhler number scaling of active cascade effects in turbulent premixed combustion," Phys. Fluids **33**, 035103 (2021).
[9]N. Chakraborty, C. Kasten, U. Ahmed, and M. Klein, "Evolutions of strain rate and dissipation rate of kinetic energy in turbulent premixed flames," Phys. Fluids **33**, 125132 (2021).
[10]A. N. Lipatnikov and J. Chomiak, "Effects of premixed flames on turbulence and turbulent scalar transport," Prog. Energy Combust. Sci. **36**, 1 (2010).
[11]V. A. Sabelnikov and A. N. Lipatnikov, "Recent advances in understanding of thermal expansion effects in premixed turbulent flames," Annu. Rev. Fluid Mech. **49**, 91 (2017).
[12]N. Chakraborty, "Influence of thermal expansion on fluid dynamics of turbulent premixed combustion and its modeling implications," Flow Turbul. Combust. **106**, 753 (2021).
[13]A. M. Steinberg, P. E. Hamlington, and X. Zhao, "Structure and dynamics of highly turbulent premixed combustion," Prog. Energy Combust. Sci. **85**, 100900 (2021).
[14]P. E. Hamlington, A. Y. Poludnenko, and E. S. Oran, "Interactions between turbulence and flames in premixed reacting flows," Phys. Fluids **23**, 125111 (2011).
[15]B. Bobbitt, S. Lapointe, and G. Blanquart, "Vorticity transformation in high Karlovitz number premixed flames," Phys. Fluids **28**, 015101 (2016).

[16]B. Bobbitt and G. Blanquart, "Vorticity isotropy in high Karlovitz number premixed flames," Phys. Fluids **28**, 105101 (2016).

[17]S. H. R. Whitman, C. A. Z. Towery, A. Y, Poludnenko, and P. E. Hamlington, "Scaling and collapse of conditional velocity structure functions in turbulent premixed flames," Proc. Combust. Inst. **37**, 2527 (2019).

[18]J. Lee, J. F. MacArt, M. E. Mueller, "Heat release effects on the Reynolds stress budgets in turbulent premixed jet flames at low and high Karlovitz numbers," Combust. Flame **216**, 1 (2020).

[19]R. Darragh, C . A. Z. Towery, A. Y. Poludnenko, and P. E. Hamlington, "Particle pair dispersion and eddy diffusivity in a high-speed premixed flame," Proc. Combust. Inst. **38**, 2845 (2021).

[20]J. Lee and M. E. Mueller, "Closure modeling for the conditional Reynolds stresses in turbulent premixed combustion," Proc. Combust. Inst. **38**, 3031 (2021).

[21]V. A. Sabelnikov, A. N. Lipatnikov, S. Nishiki, H. L. Dave, F. E. Hernández-Pérez, W. Song, and H. G. Im, "Dissipation and dilatation rates in premixed turbulent flames," Phys. Fluids **33**, 035112 (2021).

[22]A. Kazbekov and A. M. Steinberg, "Flame- and flow-conditioned vorticity transport in premixed swirl combustion," Proc. Combust. Inst. **38**, 2949 (2021).

[23]A. Kazbekov and A. M. Steinberg, "Physical space analysis of cross-scale turbulent kinetic energy transfer in premixed swirl flames," Combust. Flame **229**, 111403 (2021).

[24]V. A. Sabelnikov, A. N. Lipatnikov, S. Nishiki, and T. Hasegawa, "Application of conditioned structure functions to exploring influence of premixed combustion on two-point turbulence statistics," Proc. Combust. Inst. **37**, 2433 (2019).

[25]V. A. Sabelnikov, A. N. Lipatnikov, S. Nishiki, and T. Hasegawa, "Investigation of the influence of combustion-induced thermal expansion on two-point turbulence statistics using conditioned structure functions," J. Fluid Mech. **867**, 45 (2019).

[26]P. Brearley, U. Ahmed, N. Chakraborty, and A. Lipatnikov, "Statistical behaviors of conditioned two-point second-order structure functions in turbulent premixed flames in different combustion regimes," Phys. Fluids **31**, 115109 (2019).

[27]A. J. Chorin and J. E. Marsden, *A Mathematical Introduction to Fluid Mechanics* (Springer, Berlin, Germany, 1993).

[28]V. A. Sabelnikov, A. N. Lipatnikov, N. Nikitin, S. Nishiki, and T. Hasegawa, "Application of Helmholtz-Hodge decomposition and conditioned structure functions to exploring influence of premixed combustion on turbulence upstream of the flame," Proc. Combust. Inst. **38**, 3077 (2021).

[29]D. H. Wacks, N. Chakraborty, M. Klein, P. G. Arias, and H. G. Im, "Flow topologies in different regimes of premixed turbulent combustion: A direct numerical simulation analysis," Phys. Rev. Fluids **1**, 083401 (2016).

[30]A. N. Lipatnikov, V. A. Sabelnikov, F. E. Hernández-Pérez, W. Song, and H. G. Im, "A priori DNS study of applicability of flamelet concept to predicting mean concentrations of species in turbulent premixed flames at various Karlovitz numbers," Combust. Flame **222**, 370 (2020).

[31]A. N. Lipatnikov, V. A. Sabelnikov, F. E. Hernández-Pérez, W. Song, and H. G. Im, "Prediction of mean radical concentrations in lean hydrogen-air turbulent flames at different Karlovitz numbers adopting a newly extended flamelet-based presumed PDF," Combust. Flame **226**, 248 (2021).

[32]H. Bhatia, G. Norgard, V. Pascucci, and P.-T. Bremer, "The Helmholtz-Hodge decomposition – a survey," IEEE Trans. Vis. Comput. Graph. **19**, 1386 (2013).

[33]H. Bhatia, V. Pascucci, and P.-T. Bremer, "The natural Helmholtz-Hodge decomposition for open-boundary flow analysis," IEEE Trans. Vis. Comput. Graph. **20**, 1566 (2014).

[34]V. A. Sabelnikov, A. N. Lipatnikov, N. Nikitin, S. Nishiki, and T. Hasegawa, "Solenoidal and potential velocity fields in weakly turbulent premixed flames," Proc. Combust. Inst. **38**, 3087 (2021).

[35]A. S. Monin and A. M. Yaglom, *Statistical Fluid Mechanics: Mechanics of Turbulence*, vol. 2 (MIT Press, Cambridge, Massachusetts, 1971).

[36]A. N. Kolmogorov, "Local structure of turbulence in an incompressible fluid at very high Reynolds numbers," Dokl. Akad. Nauk SSSR **30**, 299 (1941).

[37]M. Lesieur, O. Metais, and P. Comte, *Large-Eddy Simulations of Turbulence* (Cambridge University Press, Cambridge, U.K., 2005).

[38] M. P. Burke, M. Chaos, Y. Ju, F. L. Dryer, and S. J. Klippenstein, “Comprehensive H_2/O_2 kinetic model for high-pressure combustion,” Int. J. Chem. Kinet. **44**, 444 (2012).

[39] R. S. Rogallo, Numerical experiments in homogeneous turbulence, NASA Technical Memorandum 81315, NASA Ames Research Center, California, 1981.

[40] T. Passot and A. Pouquet, “Numerical simulation of compressible homogeneous flows in the turbulent regime,” J. Fluid Mech. **181**, 441 (1987).

[41] N. Peters, *Turbulent Combustion* (Cambridge Univ. Press, Cambridge, UK, 2000).

[42] Ya. B. Zel'dovich, G. I. Barenblatt, V. B. Librovich, and G. M. Makhviladze, *The Mathematical Theory of Combustion and Explosions* (Consultants Bureau, New York, 1985).

[43] Y. A. Gostintsev, A. G. Istratov, and Y. V. Shulenin, “Self-similar propagation of a free turbulent flame in mixed gas mixtures,” Combust. Explos. Shock Waves **24**, 563 (1988).

[44] B. D. Videto and D. A. Santavicca, D.A., “Flame-turbulence interactions in a freely-propagating, premixed flame,” Combust. Sci. Technol. **70**, 47 (1990).

[45] J. Furukawa, Y. Noguchi, T. Hirano, and F. Williams, “Anisotropic enhancement of turbulence in large-scale, low-intensity turbulent premixed propane-air flames,” J. Fluid Mech. **462**, 209 (2002).

PLEASE CITE THIS ARTICLE AS DOI: 10.1063/5.0096509

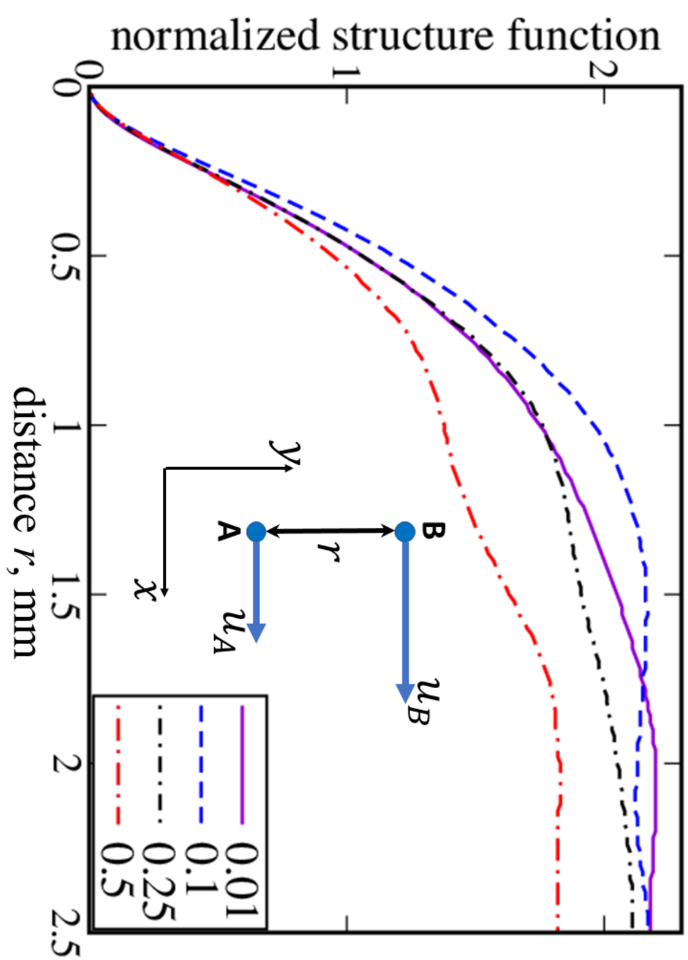

PLEASE CITE THIS ARTICLE AS DOI: 10.1063/5.0096509

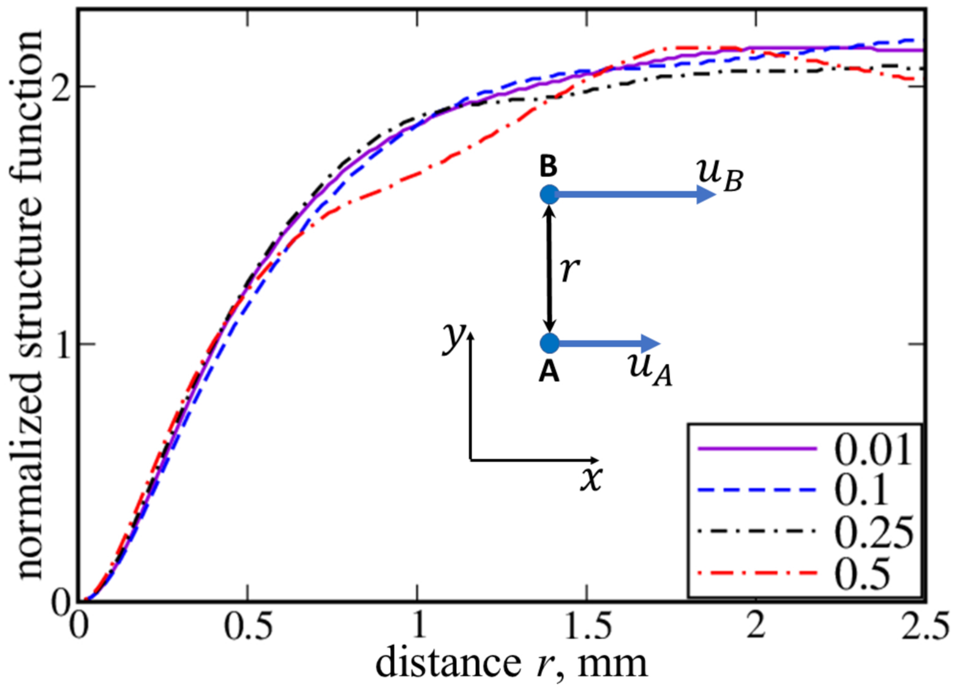

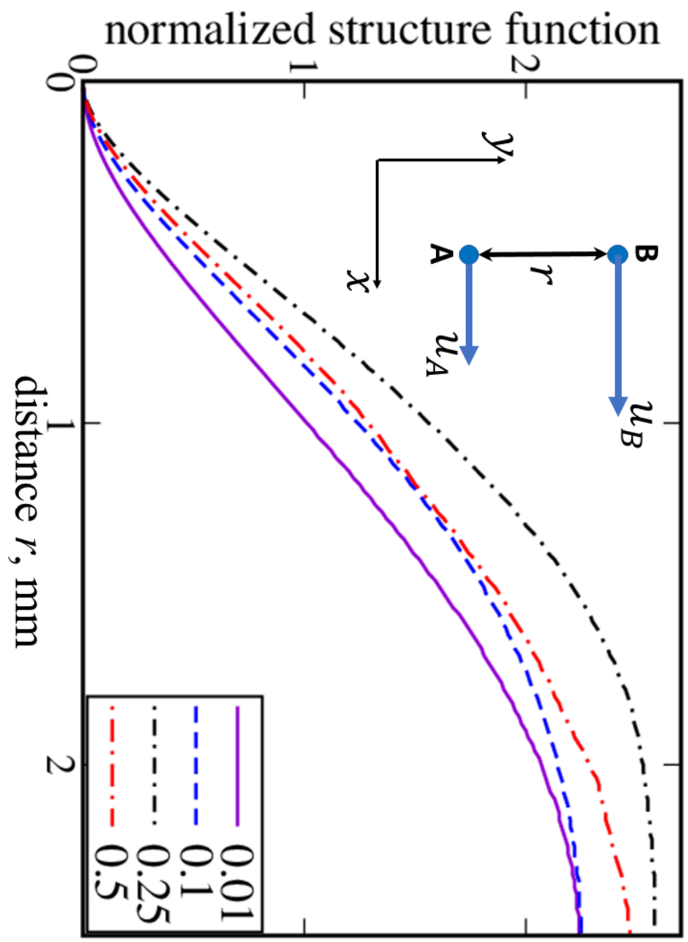
normalized structure function
distance r, mm
0
1
2
0
1
2
B
A
r
y
x
u_B
u_A
0.01
0.1
0.25
0.5

PLEASE CITE THIS ARTICLE AS DOI: 10.1063/5.0096509

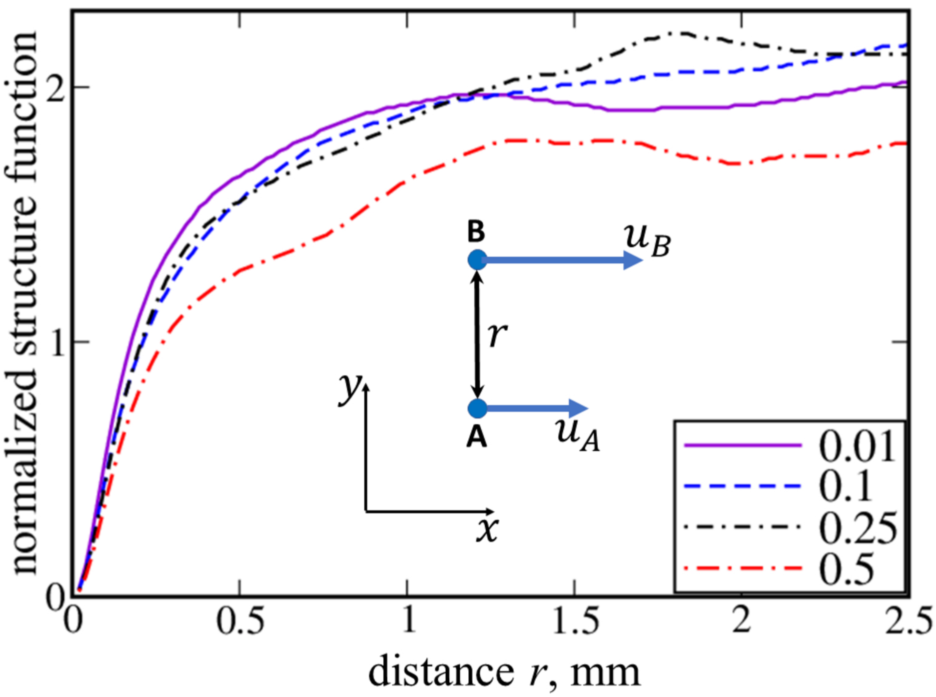

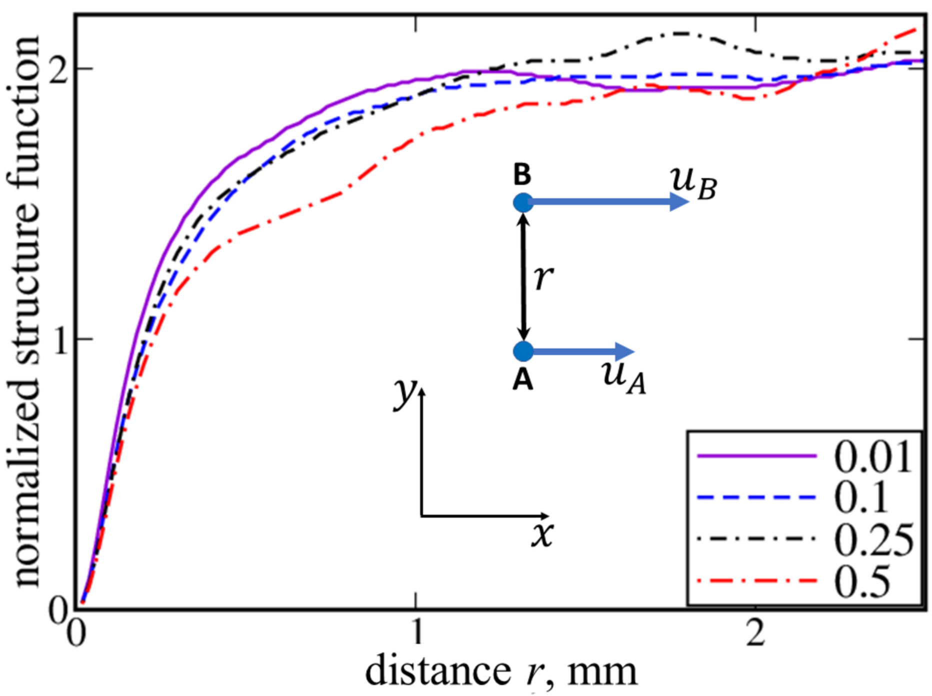
normalized structure function
distance r, mm
0
1
2
B
A
u_B
u_A
r
y
x
0.01
0.1
0.25
0.5

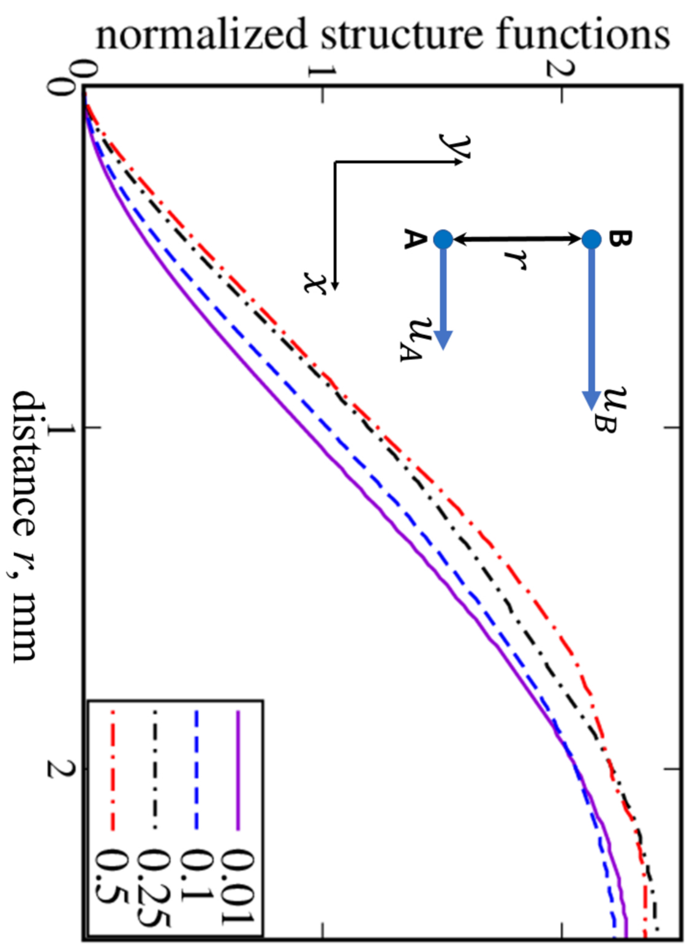
normalized structure functions
distance r, mm
0
1
2
B
A
r
y
x
u_A
u_B
0.01
0.1
0.25
0.5

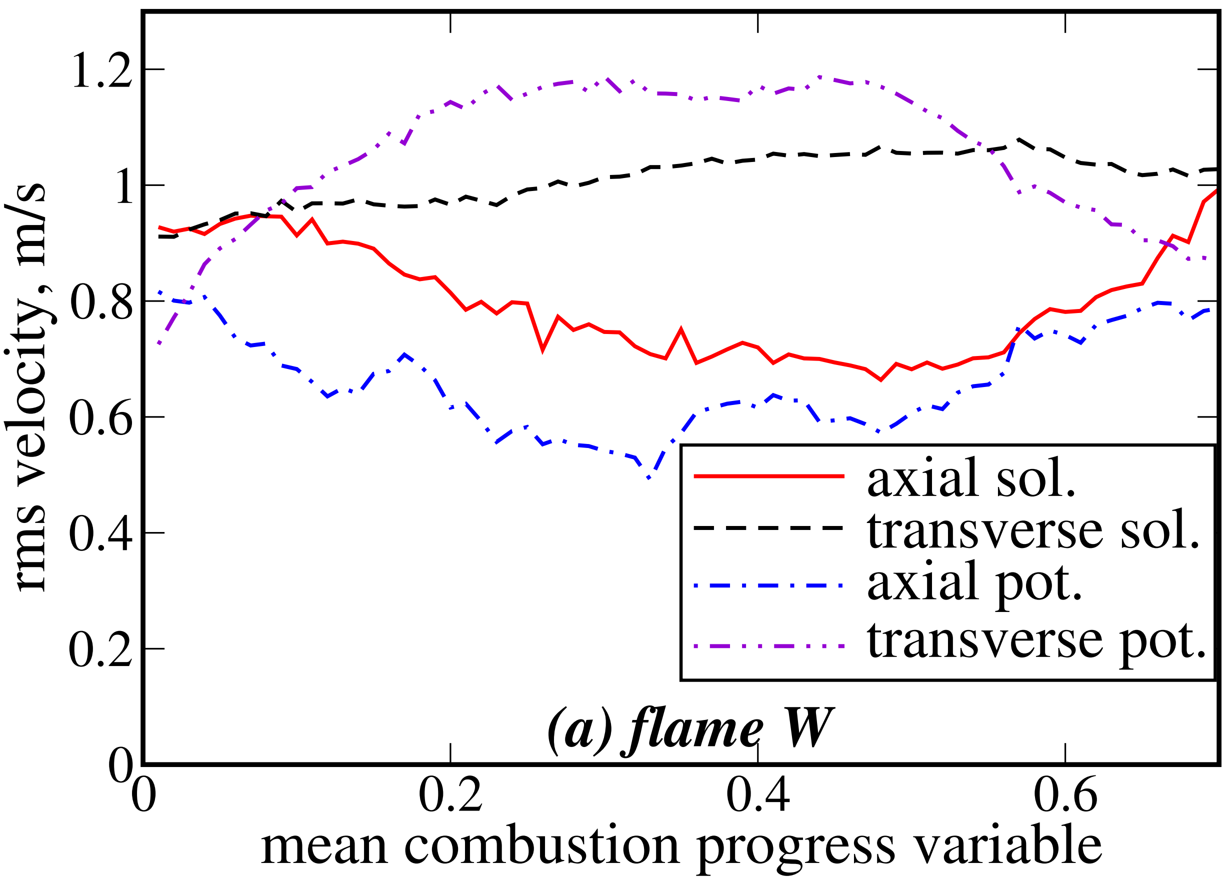
rms velocity, m/s
1.2
1
0.8
0.6
0.4
0.2
0
axial sol.
transverse sol.
axial pot.
transverse pot.
(a) flame W
0
0.2
0.4
0.6
mean combustion progress variable

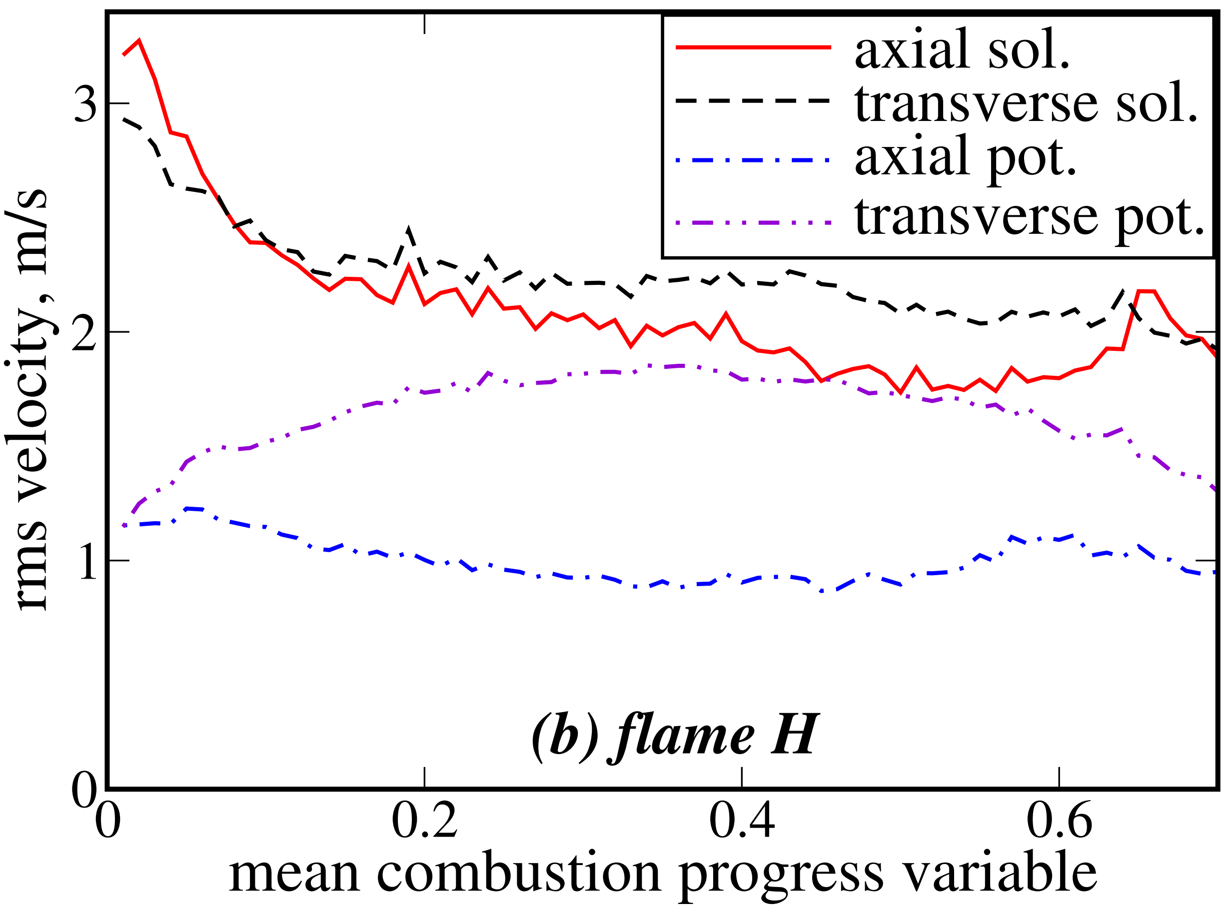
axial sol.
transverse sol.
axial pot.
transverse pot.
rms velocity, m/s
0
1
2
3
0
0.2
0.4
0.6
mean combustion progress variable
(b) flame H

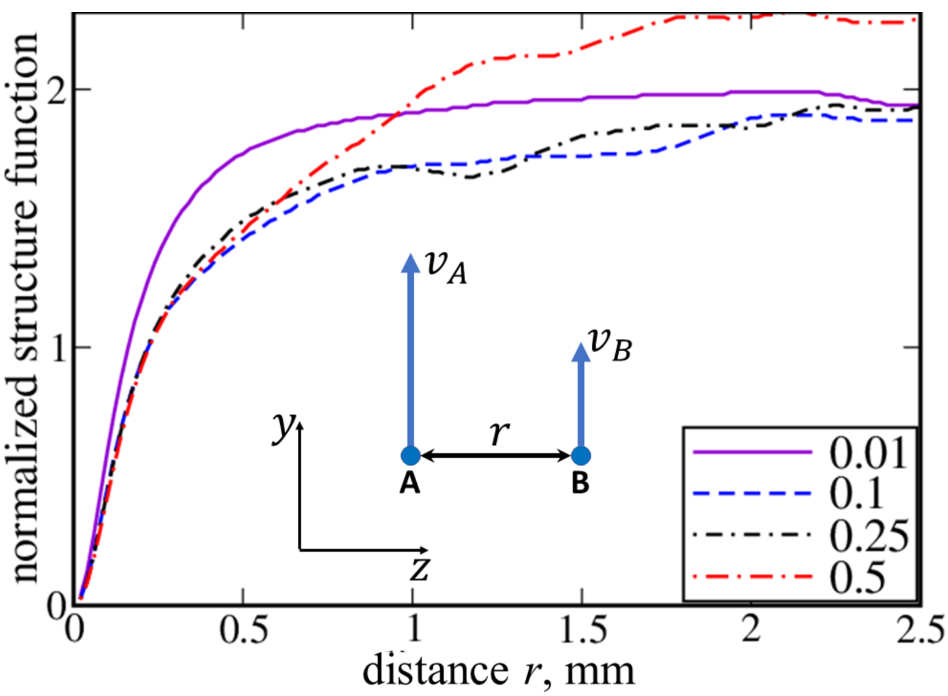
normalized structure function
distance r, mm
0
0.5
1
1.5
2
2.5
0
1
2
v_A
v_B
r
A
B
y
z
0.01
0.1
0.25
0.5

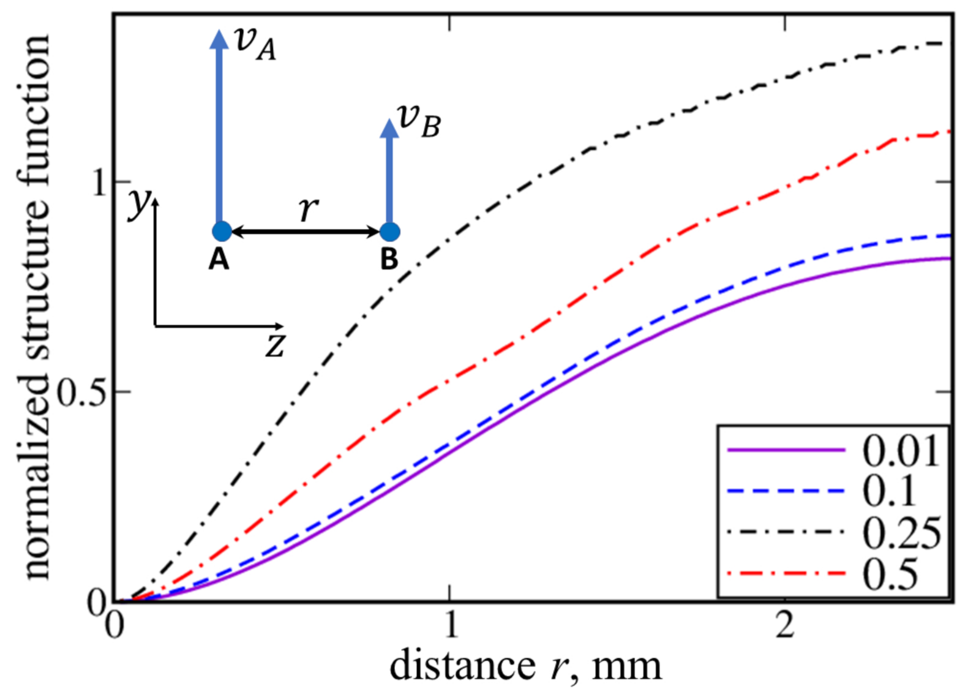
v_A
v_B
y
r
A
B
z
normalized structure function
0
0.5
1
0
1
2
distance r, mm
0.01
0.1
0.25
0.5

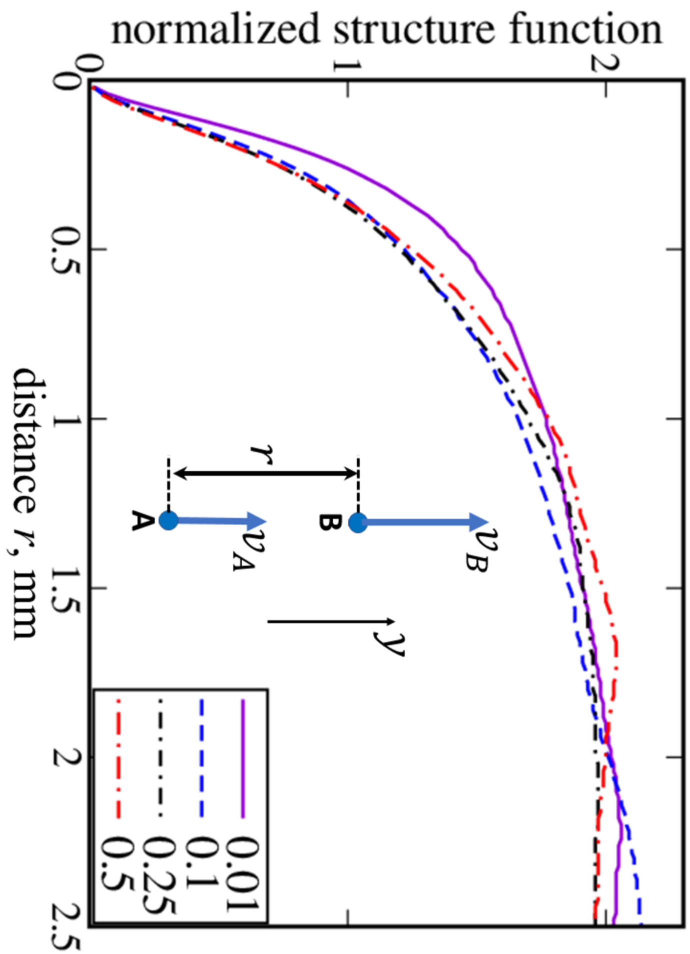
normalized structure function
distance r, mm
0
0.5
1
1.5
2
2.5
0
1
2
r
v_A
v_B
A
B
y
0.01
0.1
0.25
0.5

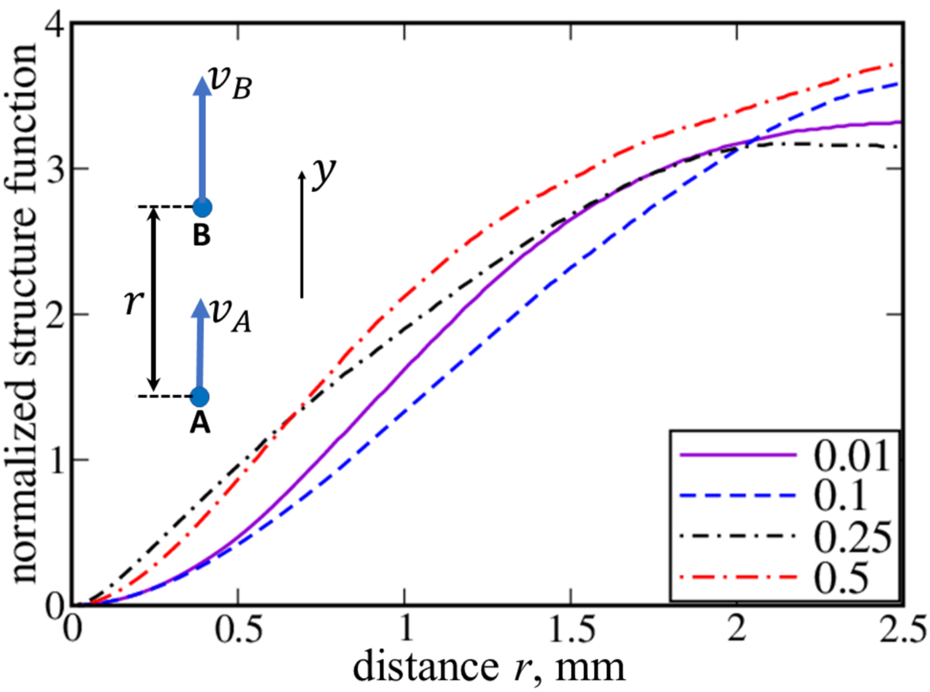
normalized structure function
distance r, mm
0
0.5
1
1.5
2
2.5
1
2
3
4
v_B
v_A
B
A
r
y
0.01
0.1
0.25
0.5

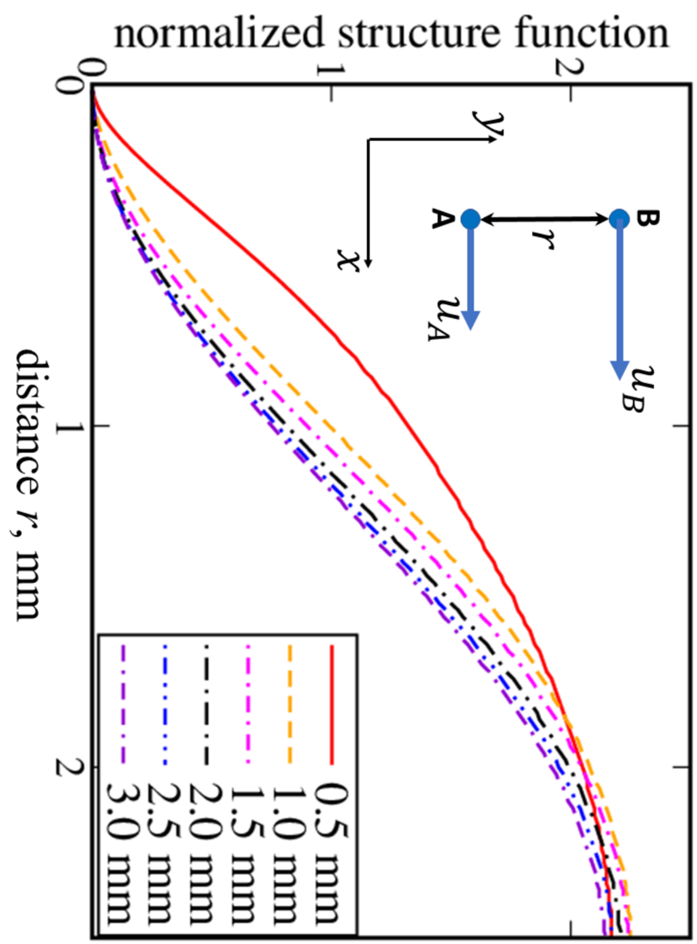
normalized structure function
distance r, mm
0
1
2
B
A
u_B
u_A
r
y
x
0.5 mm
1.0 mm
1.5 mm
2.0 mm
2.5 mm
3.0 mm

PLEASE CITE THIS ARTICLE AS DOI: 10.1063/5.0096509

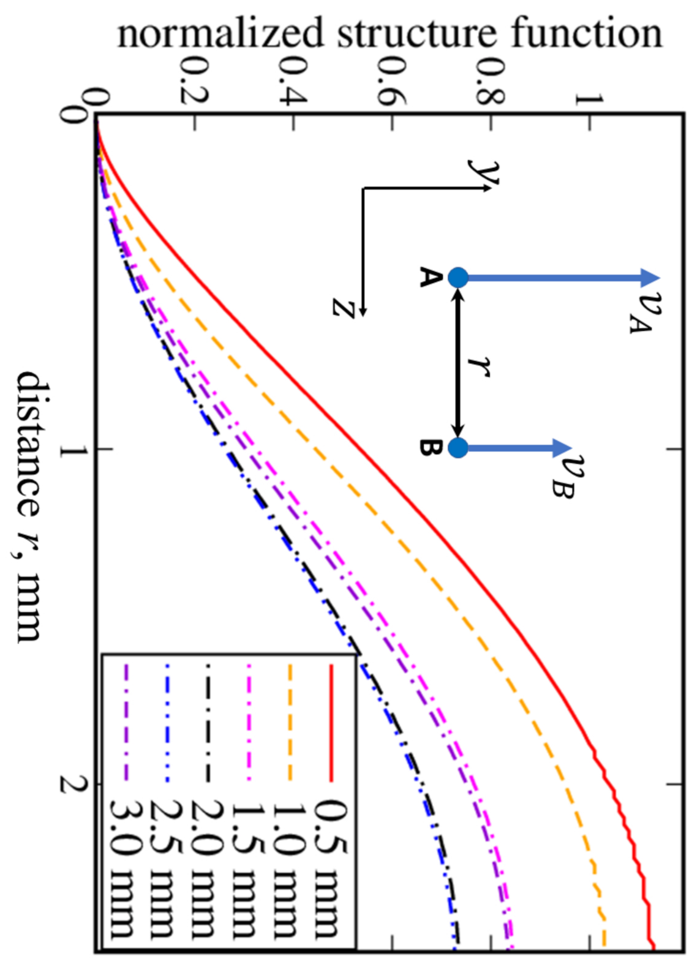

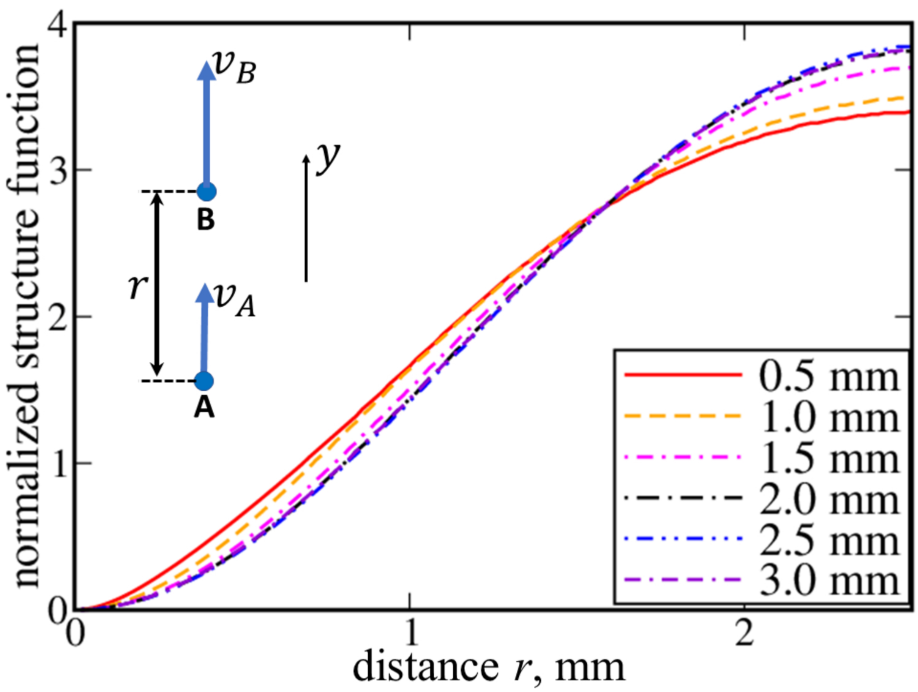
normalized structure function
distance r, mm
0
1
2
3
4
0.5 mm
1.0 mm
1.5 mm
2.0 mm
2.5 mm
3.0 mm
A
B
r
y

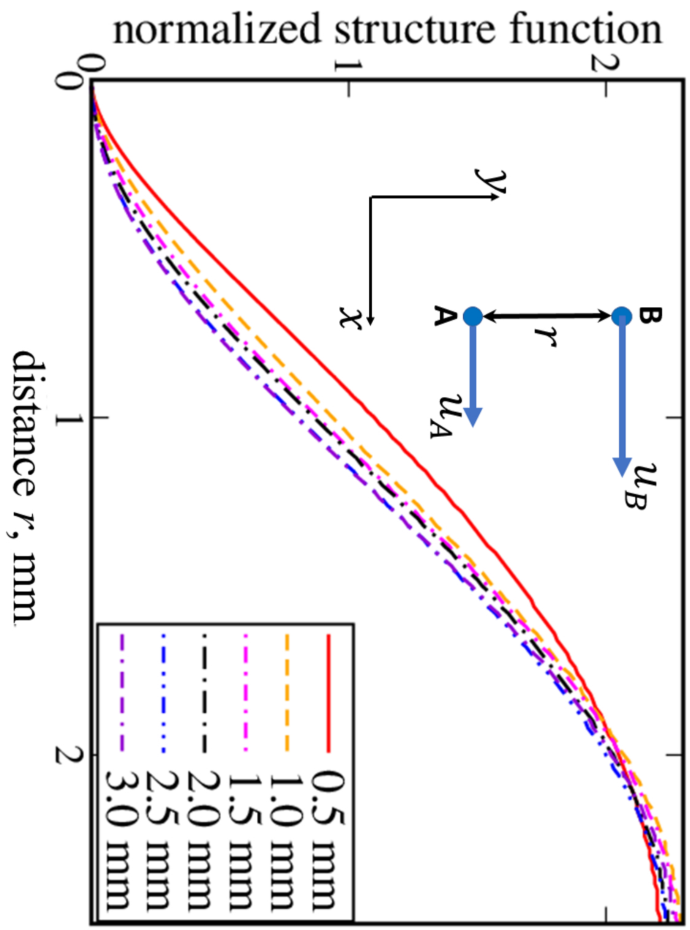
normalized structure function
distance r, mm
B
A
u_B
u_A
r
x
y
0.5 mm
1.0 mm
1.5 mm
2.0 mm
2.5 mm
3.0 mm

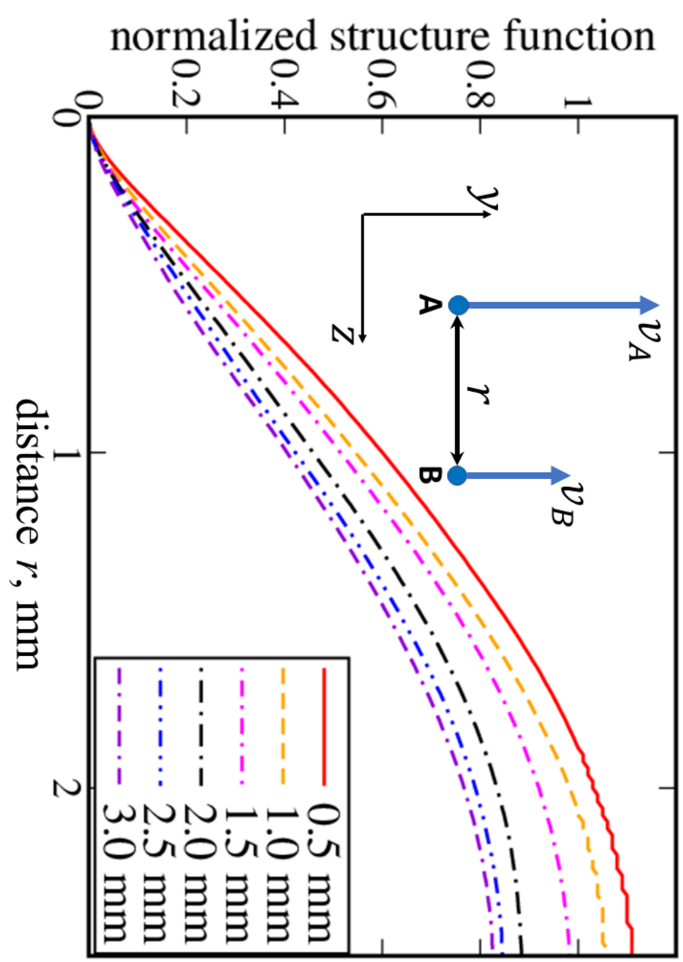
normalized structure function
distance r, mm
0
0.2
0.4
0.6
0.8
1
2
y
z
A
B
r
v_A
v_B
0.5 mm
1.0 mm
1.5 mm
2.0 mm
2.5 mm
3.0 mm

PLEASE CITE THIS ARTICLE AS DOI: 10.1063/5.0096509

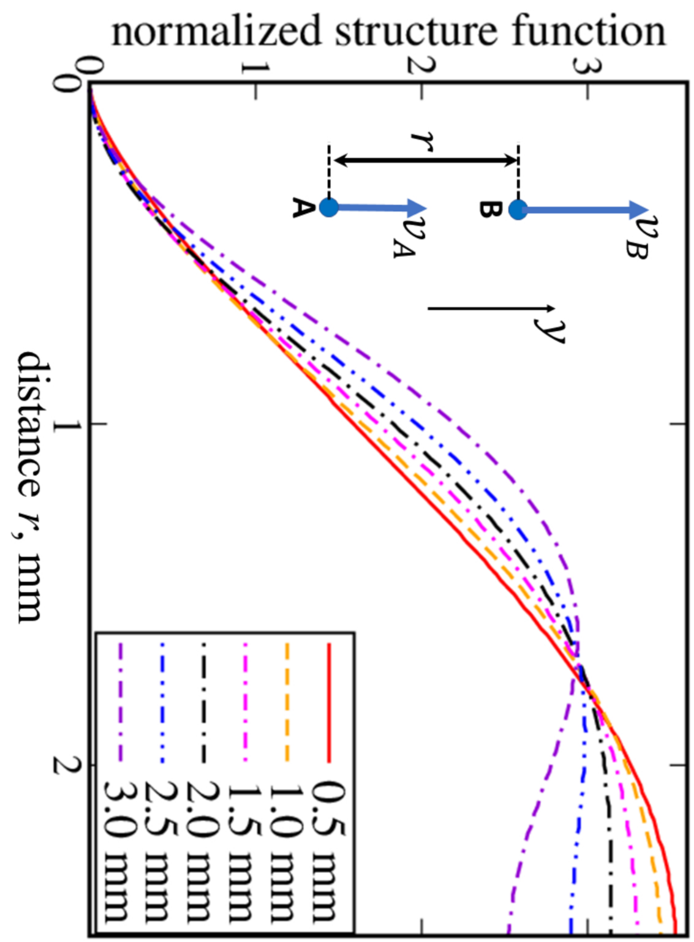

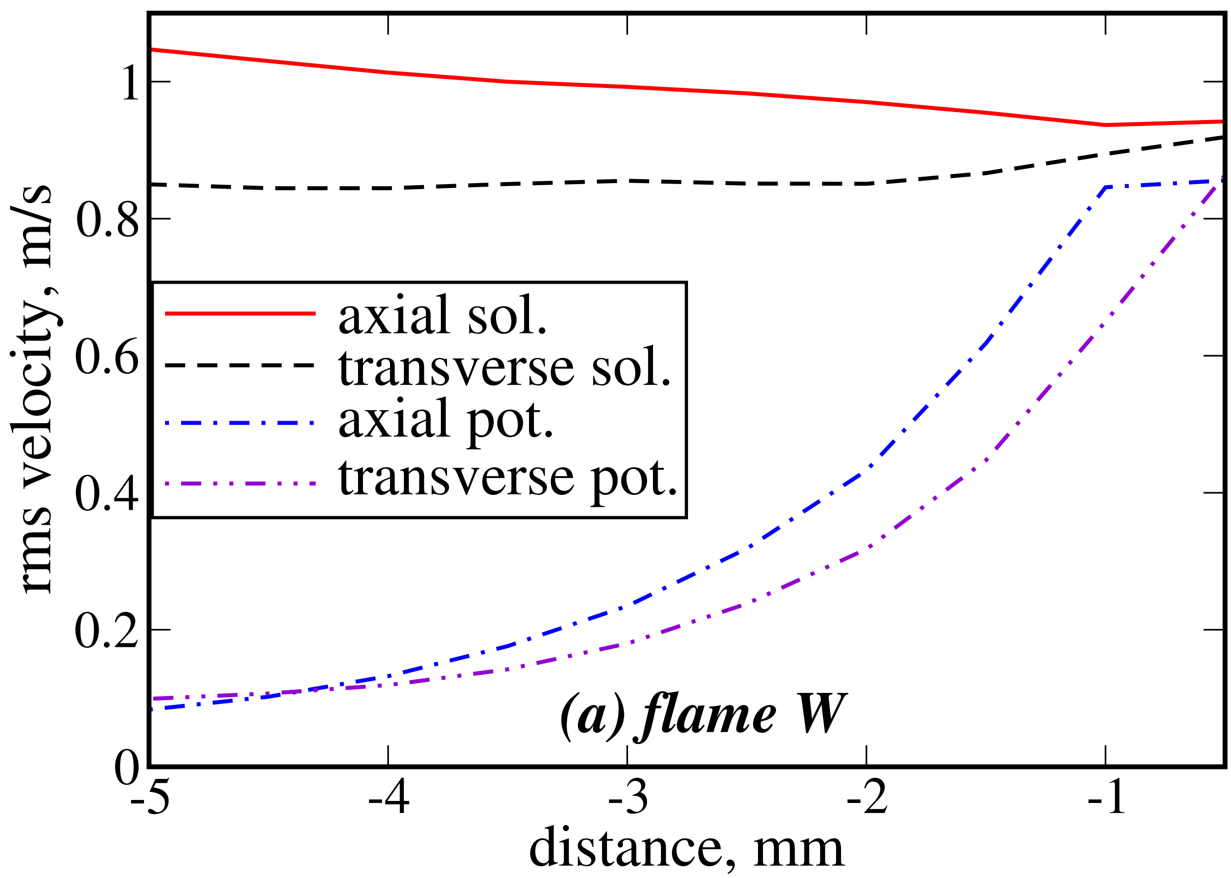
rms velocity, m/s
0
0.2
0.4
0.6
0.8
1
-5
-4
-3
-2
-1
distance, mm
axial sol.
transverse sol.
axial pot.
transverse pot.
(a) flame W

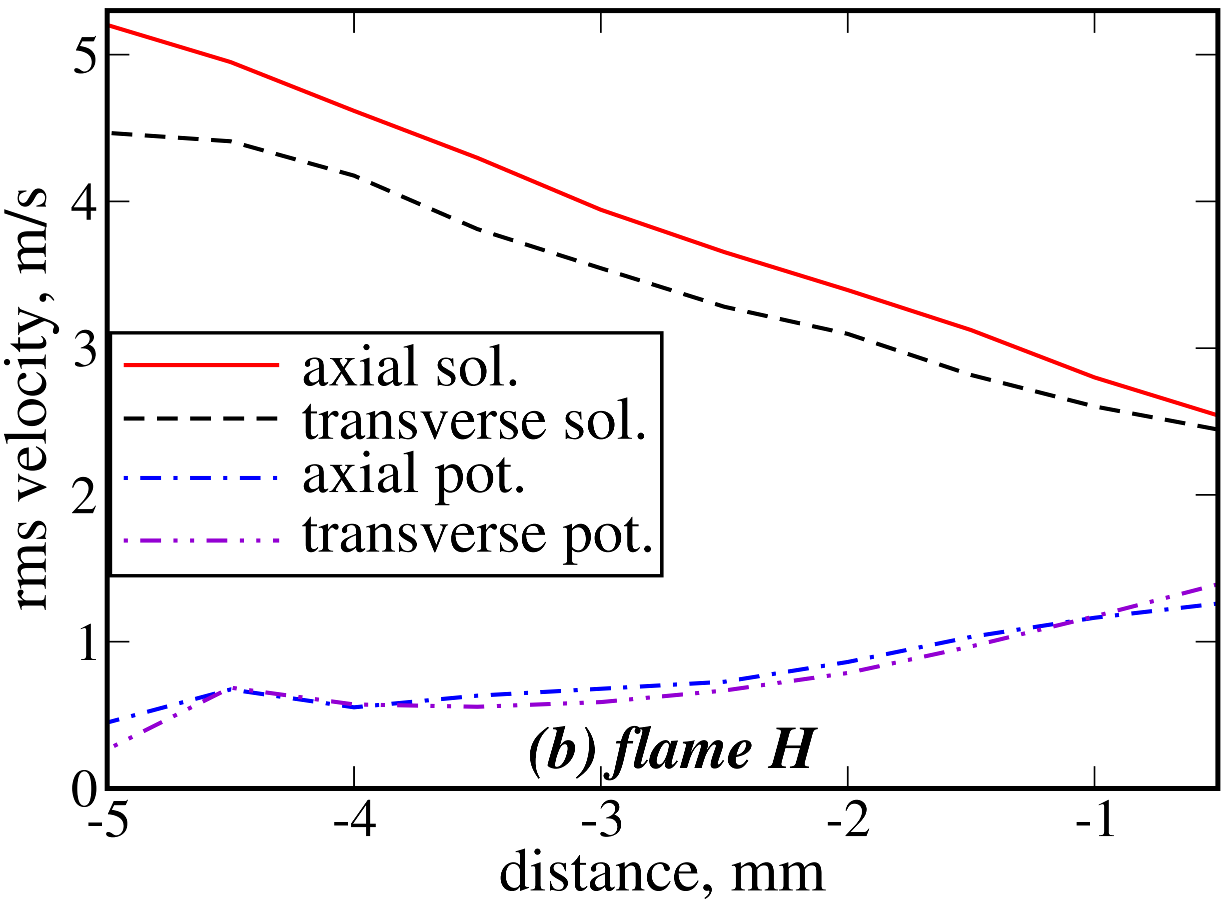
rms velocity, m/s
distance, mm
0
1
2
3
4
5
-5
-4
-3
-2
-1
axial sol.
transverse sol.
axial pot.
transverse pot.
(b) flame H

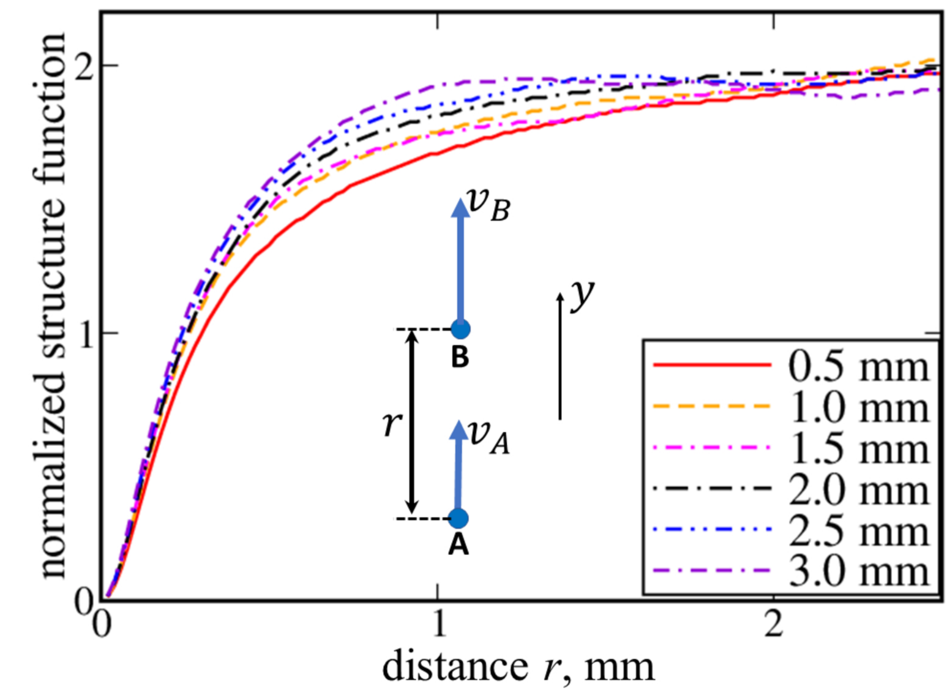
normalized structure function
distance r, mm
0
1
2
0
1
2
v_B
v_A
B
A
r
y
0.5 mm
1.0 mm
1.5 mm
2.0 mm
2.5 mm
3.0 mm